Investigation of minimum driving force for the dye regeneration utilizing model squaraine dyes for dye-sensitized solar cells

Anusha Pradhan*, Takuya Morimoto, Maryala Saikiran, Gaurav Kapil, Shuzi Hayase and Shyam S. Pandey*

Combined theoretical and experimental approaches have been implemented to design model far-red sensitive unsymmetrical squaraine dyes in order to estimate the minimum energy barrier required for the facile dye regeneration. Our logical molecular design indicates that it is possible to have a fine control on the energetics within 0.2 eV only by judicious selection of substituents and alkyl chain length keeping main p-molecular framework the same. Utilization of LSDA functional under TD-DFT calculations offers an effective and cost effective computation method for the reliable prediction the energetics as well as absorption maximum the sensitizers used for present research. Amongst the designed dyes under investigation, SQ-75 exhibited best photovoltaic performance having a short-circuit current density of 10.92 mA/cm2, open circuit voltage of 0.57 V and a fill factor of 0.67 leading to an efficiency of 4.25 % in spite of having photon harvesting mainly in the far-red region. Best photon harvesting by SQ-75 even with an energy difference of only 0.12 eV between the energy of its highest occupied molecular orbital and redox energy level I^-/I_3^- electrolyte corroborates the facile dye regeneration with such a small driving force.

1. Introduction

Growing demands for energy due to ever increasing world population and standard of human life have increased the fast pace utilization of fossil fuels as a major energy resources. This has not only led to the fast depletion of precious non-renewable energy resources but also enhanced greenhouse gas emission leading to the danger of global warming (1). This has imposed an urgent need for the implementation and utilization of renewable energy resources and solar energy seems to be one of the amicable solutions owing to its vast availability as free gift from the nature (2). Implementation of solar cells is undoubtedly an important strategy to harness this immensely available light energy in to directly usable electricity. Dye-sensitized solar cells (DSSCs) have emerged as one of the important candidates amongst next generation solar cells owing to its ease of fabrication, economic viability and environment friendly solar energy harvesting (3). Research and development carried out in the past two decades have led to the achievement of the photoconversion efficiency (PCE) over 12% surpassing the commercially available amorphous silicon solar cells (4). This has become possible by the optimization of various components such as wide band gap mesoporous semiconductor, potential photosensitizers, redox electrolyte and counter electrodes (5-8).

Sensitizing dyes play a pivotal role in controlling the overall external PCE since it is directly involved in the trapping of photons from sun light. It is remarkable to see that the utilization of some potential sensitizers in DSSCs has led to the attainment of PCE beyond 12 % even having photon harvesting mainly in the visible wavelength region from 400 nm to 750 nm (9-10). This has imposed an urgent need for the logical design and development of sensitizers having the capability of photon harvesting in the near infra-red (NIR)-IR wavelength region. A panchromatic photon harvesting is, therefore, highly desired by implementing novel NIR sensitizers in combination with the already developed potential visible dyes for further enhancement in the external PCE. These two kinds of dyes can be easily incorporated in to DSSCs by adopting hybrid or tandem device architectures (11-14). In past, efforts have been already directed for the design and development of far-red and NIR sensitizers with successful far-red photosensitization but unfortunately efficient photon harvesting in the NIR wavelength region of spectrum are yet to be achieved (15-16).

Apart from the wide wavelength photon harvesting, sensitizing dyes must possess energetic cascade with the electron accepting wide band gap semiconductor and redox electrolyte in order to have facile electron injection and dye regeneration, respectively. In this respect, design and development of efficient NIR dyes are rather more challenging due to their relatively smaller band gap (Eg). This small Eg of NIR sensitizers imposes strict control of the energetics for their optimal functioning and a judicious molecular design is highly desired. At the same time, it becomes very important to know the minimum possible energy barrier for both of the electron injection as well as the dye regeneration. Such a knowledge about this energy barrier offsets will help to design novel sensitizers having maximum possible wavelength window for

a given set of mesoporous wide band gap semiconductor and redox electrolyte. Using model squaraine dyes, we have recently demonstrated that it is possible to control the energetics by 0.1 eV simply by changing the substituents keeping the main π-conjugated framework the same, only by the alteration of alkyl chain length (17). At the same time, we have also reported that it is possible to have electron injection from lowest unoccupied molecular orbital (LUMO) of photoexcited dye to conduction band of TiO_2 with the energy barrier as small as 0.16 eV (18).

State-of-art theoretical calculations using Gaussian program package have been extensively utilized to facilitate the design and development of novel sensitizers in the recent past (19). Theoretical prediction of energy of dye molecules in the ground and excited states along with the electronic absorption spectra is highly desired in order to accelerate the development of potential sensitizers. Based on our combined theoretical and experimental approaches, we have recently shown that a logical selection of basis set and functional under time-dependent density functional theory (TD-DFT), it is possible to minimize the error between theoretically calculated and experimentally observed values of energetics and electronic absorption maximum (λ_{max}) (20). Present investigation deals with the estimation of minimum possible energy barrier for dye regeneration of the oxidised dye from most widely used iodine based (I^-/I_3^-) redox electrolyte using some model unsymmetrical far-red sensitive squaraine dyes with molecular structure as shown in the Fig. 1. In combination with our previously reported work on minimum energy barrier for the electron injection, results obtained in this work are expected to the synergistically accelerate the development novel NIR sensitizers. Apart from the theoretical calculation on the dyes shown in the Fig. 1, they were synthesized, characterized and subjected to the photophysical investigations also to correlate the theoretical results with the experimentally obtained values. Calculated results on energy of molecules in the ground and excited states, band gap, λ_{max} for these molecules were then compared with experimentally observed values to find the optimum molecular structure with smallest driving force for dye regeneration.

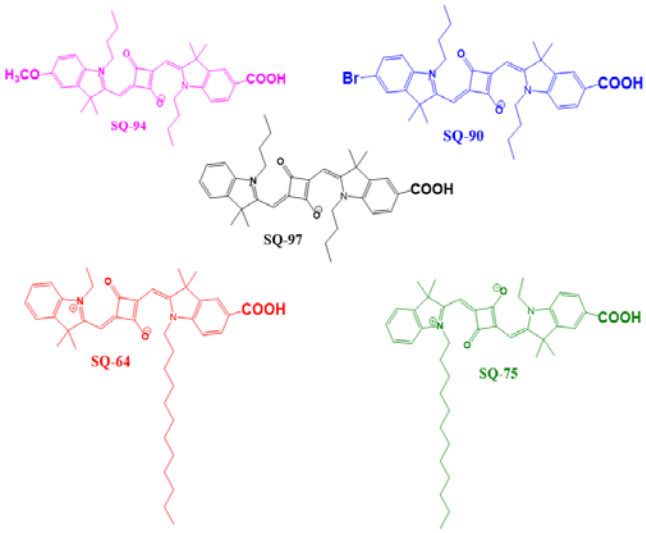

Figure 1. Molecular structure of unsymmetrical squaraine dyes used for present investigation.

2. Experimental

2.1 Materials and Methods

All of the chemicals and solvents used in this work are of analytical/spectroscopic grade and used as received without any further purification. Synthesized final dyes and their respective intermediates were analysed by high performance liquid chromatography (HPLC) for purity. Matrix assisted laser desorption and ionization (MALDI)-time-of-flight (TOF)-mass and fast ion bombardment (FAB)-mass spectrometry in the positive ion monitoring mode and nuclear magnetic resonance (NMR) spectroscopy (JEOL, 500 MHz) were utilized for structural elucidation. Electronic absorption spectra of the dyes in ethanol solution as well as in thin films for the dyes adsorbed on TiO_2 were measured using UV–visible-NIR spectrophotometer (JASCO model V550). Energy band diagram for the dyes were constructed after estimating the energy of highest occupied molecular orbital (HOMO), Energy band gap (Eg) and energy of their LUMO. HOMO energy level of the sensitizing dyes was estimated using photoelectron yield spectroscopy (Bunko Keiki, model KV-205 HK, Japan). LUMO energy level was estimated using the relation LUMO = HOMO + Eg, where, Eg is the optical band gap. Eg was estimated from the energy corresponding to the $E_{o\text{-}o}$ transition which was the considered at cross-section wavelength of the dye for its electronic absorption and fluorescence emission spectrum. Fluorescence lifetime of the dyes in the ethanol solution was measured using fluorescence lifetime measurement system (Quantarus Tau Model C-11370, Hamamatsu Photonics, Japan). Theoretical quantum chemical calculations pertaining to the structural optimization, calculation of energies of the HOMO and LUMO along with the electronic absorption spectra were conducted on Dell workstation using Gaussian G09 program package (20). Calculation was performed for the isolated single molecule in gaseous state using TD-DFT theory, 6-311 G basis set and linear spin density approximation (LSDA) as optimal functional as calculation parameters based on our previously published work (19).

DSSCs were fabricated using Ti-Nanoxide D/SP paste (Solaronix SA) which was coated on a Low E fluorine doped tin-oxide (FTO) glass (Nippon Sheet Glass Co., Ltd.) by screen printing. TiO_2 coated FTO substrate was baked at 450◦C for 30 min to fabricate TiO_2 layers of about 10 μm thickness. Substrate was then dipped in the 0.25 mM ethanolic solution of the respective dyes in the presence of 25 mM of chenodeoxycholic acid (CDCA) acting as co-absorber for 4 hours. A Pt sputtered FTO glass substrate was employed as the counter electrode. Electrolyte containing LiI (500 mM), iodine (50 mM), t-butylpyridine (580 mM), MeEtIm-DCA (ethylmethylimidazolium dicyanoimide) (4:6, wt/wt) (600mM) in acetonitrile was used to fabricate the DSSC. A hot melt polymer film (Meltonix-1170, Solaronix) of 25 μm thickness was used as a spacer.

Photovoltaic performance of the cells was measured using a solar simulator (CEP-2000 Bunko Keiki Co. Ltd, Japan) equipped with a xenon lamp (Bunko Keiki BSO-X150LC) used as a light source of simulated solar irradiation at 100 mW/cm², AM 1.5G. Power of the light exposure from the solar simulator was also adjusted with an amorphous Si photodetector (Bunko

Keiki BS-520 S/N 353) to avoid the optical mismatch between the calibration diode and the DSSCs. The photocurrent action spectrum was measured as a function of wavelength from 300 to 800 nm with a constant photon flux of 1×10^{16} photon/cm^2 at each wavelength in DC mode using the action spectrum measurement system connected to the solar simulator (CEP-2000, Bunko Keiki, Japan). Cell area was maintained precisely using a black metal mask having area of 0.2025 cm^2 during the measurement of the photovoltaic performance.

2.2 Synthesis of unsymmetrical squaraine dyes

Direct ring carboxy functionalized indole derivative 2,3,3-trimethyl-3H-indole-5-carboxylic acid (**1**) was synthesized following the method reported by Pham et al. (21). Details of the synthesis and characterization of dye intermediates (**2**) and (**3**) has been published by us previously (18). Unsymmetrical squaraine dye **SQ-64** along with its intermediates has been synthesized as per our earlier publication (22). Semi-squaraine dye intermediates (**4**, **5**, **6** and **7**) were synthesized and characterized as per our earlier publications (23). Other unsymmetrical squaraine dyes SQ-75, SQ-90, SQ-94 and SQ-97 along with their corresponding intermediate indolium iodide salts were synthesized as per the scheme shown in Fig. 2.

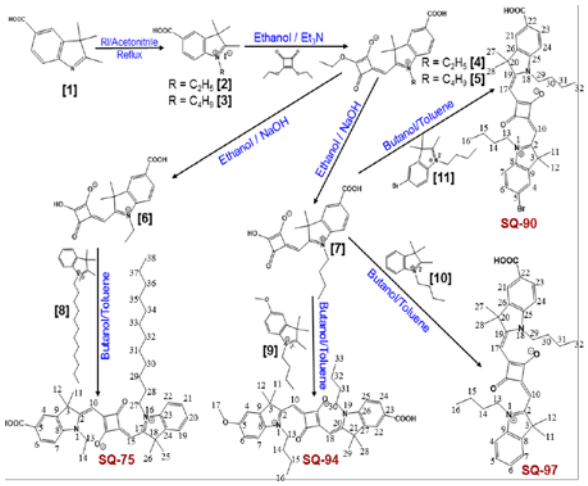

Figure 2. Synthetic route for direct –COOH functionalized unsymmetrical squaraine dyes

2.2.1 Synthesis of intermediate 2,3,3-trimethyl-1-dodecyl-3H-indolium iodide [8]

3.18 g (20mmol) of 2,3,3 trimethyl-3H-Indole and 15 mL of 1-Iododecene (60 mmol) were dissolved in 40 mL acetonitrile and then refluxed for 48 hours. Solvent was evaporated followed by addition of excess diethyl ether for precipitation. Obtained solid was filtered and washed with ether 3 times. The residue is dried under vacuum to afford 8.13 g (18 mmol) of dark pink solid as titled compound in 90% yield. HR-MS (measured m/z: 328.3013; calculated m/z: 328.2999)

2.2.2 Synthesis of intermediate 5-Methoxy-2,3,3-trimethyl-1-Butyl-3H-indolium iodide [9]

1.0 gm (5 mmol) of 5-Methoxy-2,3,3-trimethyl-3H-indole and 1.4 ml of 1-Iodobutane (10 mmol) were dissolved in 25 ml of acetonitrile and reaction mixture was heated at reflux for 36 hours (25). After completion of the reaction, solvent was evaporated and the crude product was purified by silica gel flash column using chloroform-methanol as eluting solvent. This flash column resulted in to 1.2 gm (3.21 mmol) of titled compound as purple viscous liquid in 64 % yield. MALDI-TOF mass (measured m/z: 248.0 $[M+2]^+$; calculated m/z: 246.19) confirms the synthesis of this intermediate.

2.2.3 Synthesis of intermediate 2,3,3-trimethyl-1-Butyl-3H-indolium iodide [10]

In a round bottom flask, one equivalent 2,3,3-trimethyl indole (1 eq.) and 1-Iodobutane (3 eq.) were dissolved in dehydrated acetonitrile and the reaction mixture was refluxed overnight (26). After completion of the reaction as monitored by TLC, solvent was evaporated and the crude product was washed with ample diethyl ether giving brown solid in 95% yield with 98% purity as conformed by HPLC 216.2) .confirms the successful synthesis of this intermediate.

2.2.4 Synthesis of 5-Bromo-2,3,3-trimethyl-1-Butyl-3H-indolium iodide [11]

5-Bromo-2,3,3-Trimeythyl-Indole was synthesized first before its quaternization. 4-bromophenyl hydrazine hydrochloride (8.0 gm, 35.7 mmol), 3-Methyl-2-Butanone (9.6 ml; 89 mmol) and Ethanol (60 ml) ware taken in 200 ml round bottom flask. Reaction mixture was refluxed for 2 hours under N_2 atmosphere. After completion of the condensation, ethanol was evaporated followed by addition of 100 ml of glacial acetic acid. This reaction mixture was then heated at 120^{o}C for 12 hours under N_2 atmosphere (27). Acetic acid was then removed at rotary evaporator and crude product was purified by flash silica gel column using chloroform-methanol (98:2) eluting solvent. This column purification led to the 6.5 gm (27.4 mmol) of 5-Bromo-2,3,3-Trimeythyl-Indole in the 77 % yield and >98 % purity as confirmed by HPLC. HR FAB-mass (measured m/z: 238.0 $[M]^+$; calculated m/z: 238.1).

1.8 gm (0.75 mmol) of 5-Bromo-2,3,3-trimethyl-3H-indole and 2.6 ml of 1-Iodobutane (2.25 mmol) were dissolved in 40 ml of acetonitrile and reaction mixture was heated at reflux for 24 hours. After completion of the reaction, solvent was evaporated and the crude product was washed with ample diethyl ether followed by silica gel flash column using chloroform-methanol as eluting solvent. This flash column resulted in to 2.85 gm (6.75 mmol) of titled compound as brown powder in 90 % yield having >98 % purity as confirmed by HPLC. FAB-mass (measured m/z: 295.0 $[M]^+$; calculated m/z: 295.2).

2.2.5 Synthesis of squaraine dye SQ-75

In a round bottom flask fitted with condenser, 220 mg (0.5 mmol) of 2,3,3-trimethyl-1-dodecyl-3H-indolium iodide (8) and semi-

squaraine dye intermediate (6) (164 mg, 0.5 mmol) were refluxed in the 30 ml of dehydrated benzene-butanol (1:1 v/v) mixture. Reaction mixture was heated at reflux using Dean-Stark trap for 12 hours. After the completion of reaction, solvent was evaporated and crude product was purified by silica-gel flash column chromatography using chloroform-methanol as eluting solvent. 230 mg (0.3 mmol) of final titled compound was obtained as blue solid in 99% purity as confirmed by HPLC and 72% yield. ESI- TOF mass (Calculated - 636.87 and observed – 637.39 $[M+1]^+$) along with ^1H NMR (500 MHz, d6-DMSO): d/ppm = 8.12 (d, H-19), 8.06 (dd, H-20), 7.41 (dd, H-4), 7.35 (dd, H-6), 7.21 (d, H-22), 7.05 (dd, H-21), 6.98 (dd, H-7), 6.10 (s, H-15), 6.02 (s, H-10), 4.07 (t, 2H, H-27), 4.03 (q, 2H, H-13), 1.94 (s, 6H, H-11 & H-12), 1.83 (s, 6H, H-25 & H-26), 1.25 (t, 3H, H-14), 0.87 (t, 3H, H-38) confirms the successful synthesis of the unsymmetrical squaraine dye **SQ-75**.

2.2.6 Synthesis of squaraine dye SQ-90

In a round bottom flask fitted with condenser 210 mg (0.5 mmol) of 5-bromo-1-butyl-2,3,3-trimethyl-3H-indolium iodide (**11**) and 178 mg (0.5 mmol) of semi-squaraine dye intermediate (**7**) were dissolved in 30 ml of dehydrated benzene-butanol (1:1 v/v) mixture. Reaction mixture was refluxed using Dean-Stark trap for overnight. After the completion of reaction, solvent was evaporated and crude product was purified by silica-gel flash column using chloroform-methanol as eluting solvent. 215 mg of titled compound was obtained as blue solid in 68 % yield with HPLC purity of >98 %. ESI-TOF mass (Calculated – 631.6 and observed – 632.2 $[M+2]^+$) and ^1H NMR (500 MHz, DMSO-d6): d/ppm = 8.0 (dd, H-7), 7.94 (dd, H-21), 7.82 (dd, H-23), 7.54 (dd, H-4), 7.38 (dd, H-6), 7.34 (dd, H-24), 5.85 (s, H-10), 5.83 (s, H-17), 4.09 (t, 2H, H-13), 4.07 (t, 2H, H-29), 0.94 (t, 6H, H-16 & H-32) confirms the successful synthesis of the unsymmetrical squaraine dye **SQ-90**.

2.2.7 Synthesis of squaraine dye SQ-94

In a round bottom flask fitted with condenser 187 mg (0.5 mmol) of 1-butyl-5-methoxy-2,3,3-trimethyl-3H-indolium iodide (**9**) and 178 mg (0.5 mmol) of semi-squaraine dye intermediate **(7)** were dissolved in 30 ml of dehydrated benzene-butanol (1:1 v/v) mixture. Reaction mixture was refluxed using Dean-Stark trap overnight. After the completion of reaction, solvent was evaporated and crude product was purified by silica-gel flash column chromatography using chloroform-methanol as eluting solvent. 230 mg of final titled compound was obtained as blue solid and in 79 % yield. ESI-TOF mass (Calculated – 582.74 and observed – 583.31 $[M+1]^+$) and ^1H NMR (500 MHz, DMSO-d6): d/ppm = 7.94 (dd, H-22), 7.90 (dd, H-7), 7.39 (dd, H-24), 7.27 (dd, H-4), 7.24 (dd, H-6), 6.96 (dd, H-25), 5.86 (s, H-10), 5.74 (s, H-18), 4.16 (t, 2H, H-13), 3.98 (t, 2H, H-30), 3.32 (s, 3H, H-17), 0.94 (t, 6H, H-16 & H-33) confirms the successful synthesis of the unsymmetrical squaraine dye **SQ-94.**

2.2.8 Synthesis of squaraine dye SQ-97

In a round bottom flask fitted with condenser 174 mg (0.5 mmol) of 1-butyl-2,3,3-trimethyl-3H-indolium iodide (**10**) and 178 mg (0.5 mmol) of semi-squaraine dye intermediate (**7**) were dissolved in 30 ml of dehydrated benzene-butanol (1:1 v/v) mixture. Reaction mixture was refluxed using Dean-Stark trap for overnight. After the completion of reaction, solvent was evaporated and crude product was purified by silica-gel flash column chromatography using chloroform-methanol as eluting solvent. 220 mg of final titled compound was obtained as blue solid and in 79 % yield. ESI-TOF mass (Calculated – 552.71 and observed – 553.30 $[M+1]^+$) and ^1H NMR (500 MHz, DMSO-d6): d/ppm = 7.97 (dd, H-24), 7.93 (dd, H-21), 7.57 (dd, H-23), 7.42 (d, H-7), 7.39 (dd, H-5), 7.33 (dd, H-6), 7.23 (d, H-4), 5.89 (s, H-17), 5.80 (s, H-10), 4.15 (t, 2H, H-29), 4.04 (t, 2H, H-13), 0.93 (t, 6H, H-16 & H-32) confirms the synthesis of the unsymmetrical squaraine dye **SQ-97.**

3. Results and Discussion

3.1 Optical characterizations

Squaraine dyes in general exhibit strong optical absorption in the far-red (550-700 nm) wavelength region which is attributed to the intramolecular π-π* transition along with the fluorescence emission in the visible to near IR-region (28). Electronic absorption and fluorescence emission spectra unsymmetrical squaraine synthesized in this work are shown in the Figure 3. Results of the photophysical characterizations obtained for these dyes have been summarized in Table 1.

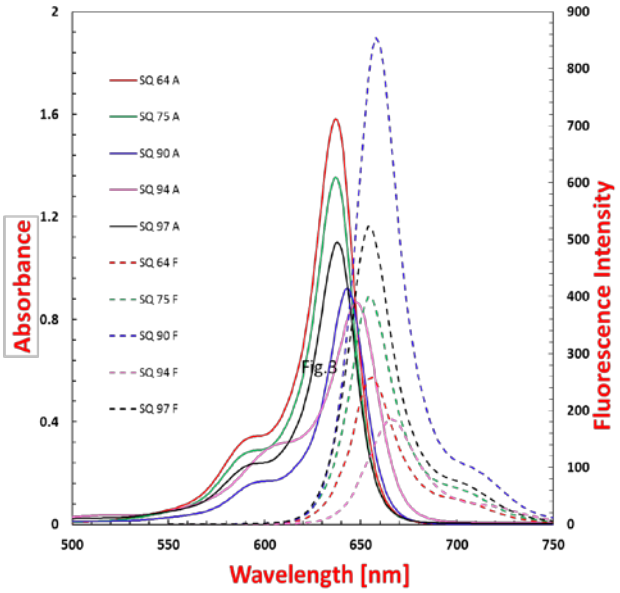

Figure 3. Solution state (5 µM) electronic absorption (solid lines) and fluorescence emission (dotted lines) spectra of squaraine dyes in ethanol solution.

A perusal of the Fig. 1 clearly indicates that all of the dyes exhibit strong light absorption mainly in the far-red region (550 nm-700 nm) of the spectrum with high molar extinction coefficient (ε) between 1.7-3.2 X 10^5 $dm^3mol^{-1}cm^{-1}$ along with the clear vibronic shoulders between 550-600 nm. Amongst dyes considered in this work, SQ-94 exhibited noticeable bathochromic shift in optical absorption maximum (λ_{max}) as well as optical absorption edge. This bathochromic shift could be attributed to the presence of electron donating methoxy group in the 5^{th} position of indole ring opposite to the indole ring bearing –COOH group.

Table 1. Experimental data for the photophysical characterization of the unsymmetrical squaraine dyes in Ethanol solution.							
Dye	Abs_{max} (nm)[a]	Em_{max} (nm)[b]	ε($dm^3mol^{-1}cm^{-1}$)	E_{o-o} (eV)[c]	Stokes shift (nm)[d]	FWHM (nm)[e]	τ (ns)[f]
SQ 64	638 (597)	656 nm	3.14 x 10^5	1.90	18	100	0.948 ± 0.004
SQ 75	638 (597)	654 nm	2.70 x 10^5	1.91	16	82	1.044 ± 0.005
SQ 90	644 (600)	660 nm	1.84 x 10^5	1.92	16	78	1.153 ± 0.006
SQ 94	648 (606)	666 nm	1.72 x 10^5	1.87	18	93	0.434 ± 0.076
SQ 97	639 (597)	656 nm	2.20 x 10^5	1.92	17	83	0.9043± 0.004

Electronic absorption[a] and fluorescence emission[b] maximum of dyes in the ethanol solution. Values of absorption maximum shown in parenthesis are obtained from the simulation absorption spectra using TD-DFT. Transition energy[c] was calculated from the wavelength of intersection of absorption and emission spectrum of corresponding dyes in ethanol. Stokes shift[d] was estimated from the separation between the absorption maximum and emission maximum. Full width at half maximum (FWHM)[e] was calculated from the electronic absorption of dyes adsorbed on TiO_2. Average fluorescence life-time (t)[f] for the dyes was calculated from transient fluorescence spectrum using time correlated single photon counting measurements.

It can also be noticed that observed Stokes shift in all of the squaraine dyes under investigation was very low (16-18 nm) indicating the conformational rigidity in other words keeping nearly similar configuration of the dye molecules in both of ground as well as the excited states [31].

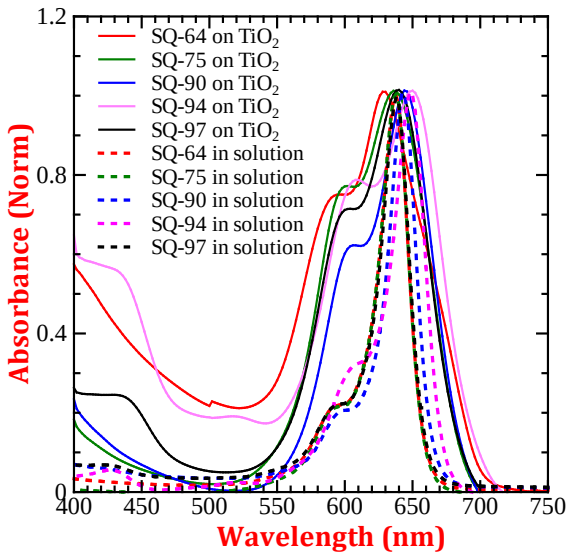

Figure 4. Normalized electronic absorption spectra in ethanol solution (dotted lines) and dyes adsorbed on to mesoporous TiO_2 (solid lines) of unsymmetrical squaraine dyes.

Normalized electronic absorption spectra of dyes adsorbed on thin film of mesoporous TiO_2 along with the corresponding results in ethanol solution has been shown in the Fig. 4. A perusal of spectral features clearly corroborates that upon adsorption of dyes on to TiO_2 surface, there is spectral broadening and increase in the full width at half-maximum (FWHM) as compared to that of the corresponding spectrum in the ethanol solution. This spectral broadening is attributed to the molecular aggregation in condensed state and interaction of carboxylic acid functional group of the dyes with the TiO_2 surface [32]. At the same time, very small vibronic shoulder in the 550-600 nm observed for dyes in solution, get highly pronounced after adsorption on to the TiO_2. This enhancement in the vibronic shoulder in squaraine dyes has been reported to be associated with dye aggregate formation and verified by its decrease in the presence of dye coadsorber like chenodeoxycholic acid [33]. It is worth to mention here that this broadening in solid-stat is more pronounced towards lower wavelength region indicating the dominance of H-aggregates. At the same time, unsymmetrical squaraine dyes SQ-64 and SQ-94 exhibit relatively pronounced absorption and clearly visible absorption peak in the 400 nm-500 nm wavelength regions which could be associated with the enhanced intermolecular interactions assisted by H-aggregate formation. In an interesting report, Kim et al have clearly demonstrated the formation of blue-shifted H-aggregates in squaraine dyes adsorbed on the SnO_2 surface [34]. H-aggregate formation by these dyes is further supported by relatively diminished fluorescence intensity (Fig. 3) in solution indicating H-aggregate assisted fluorescence quenching. Xu et al have also clearly demonstrated that H-aggregated squaraine dyes are nearly non-fluorescent and there was pronounced fluorescence turn-on upon their interaction with the bovine serum albumin [35].

3.2 Theoretical MO calculations

Quantum chemical calculations using density functional theory (DFT) has been widely utilized for the design and development of novel sensitizers for DSSC in order to have a deeper insight about energetics, electronic absorption spectra and electronic distribution [36]. Wide spread acceptance of DFT for quantum chemical calculation is due to that fact that not only it takes the account of electron and lone pair correlation like ab-initio method at diminished computation cost generally observed using Hartree-Fock method. It has been shown that its time-dependent extension (TD-DFT) give reliable results for electronic absorption spectrum using standard correlation functional implemented in the Gaussian program package [37]. Structural optimization of the squaraine

dyes under investigation were conducted using DFT, 6-311G basis set and linear spin density approximation (LSDA) functional under Gaussian G09 program. Default convergence criteria were maintained for all of the calculations during the geometry optimizations. We have previously shown that utilization of LSDA functional under DFT provides relatively more reliable results for the prediction of not only the HOMO energy level but also the λ_{max} as compared to other functional implemented under Gaussian program for squaraine dyes [38]. Electron density distribution after structural optimization in the HOMOs and LUMOs of the dyes under investigation is shown in the Fig. 5 (top). A perusal of the figure clearly corroborates that electron density in the HOMO of the dyes is mainly located on the central squaraine core while in the corresponding LUMOs, there is a clear shift of electron density distribution towards the outer indole ring bearing –COOH functional group. This seamless shift in electron density from HOMO to LUMO level is very important necessary for the facile charge transfer. At the same time, presence of sufficient electron density at anchoring group ensures the good electronic coupling between the excited dye molecules and 3d-orbital of the TiO_2 after the adsorption of dye molecules leading to the efficient interfacial injection of electrons from the excited state of the sensitizer molecule into the conduction band of the semiconductor.

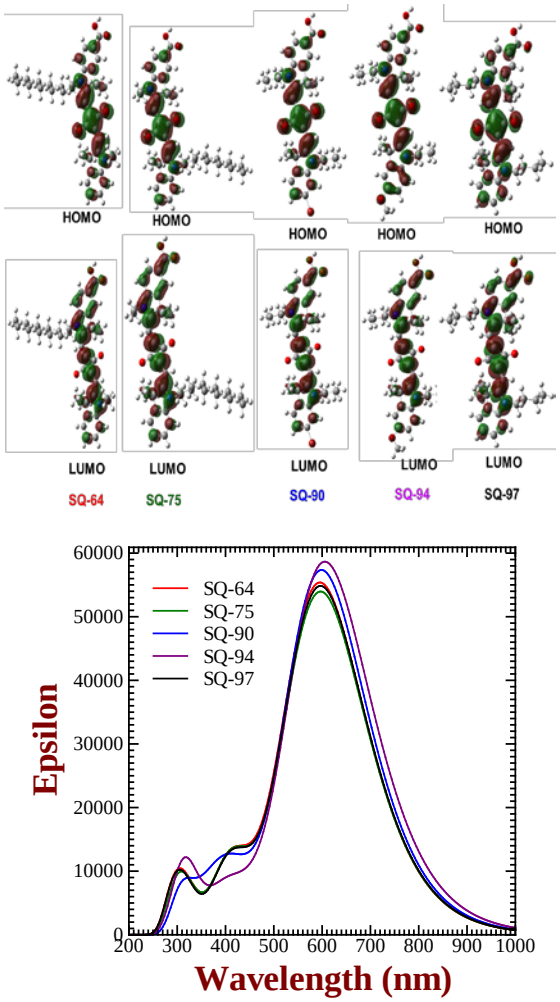

Figure 5. Calculated HOMO and LUMO orbital diagrams after structural optimization (top) and electronic absorption spectra in isolated gaseous state (bottom) for unsymmetrical squaraine dyes using LSDA functional under TD-DFT and 6-311G basis set.

It has been widely accepted that TD-DFT provides reliable predictions for the electronic excitations sensitizers used for DSSCs and accuracy of the results depends on the functional and basis set employed for the calculations [38, 39]. Fig. 5 (bottom) exhibits simulated electronic absorption spectra for the unsymmetrical squaraine dyes obtained using LSDA functional and 6-311G basis set under TD-DFT. It can be seen that simulated electronic absorption spectra exhibit distinct and strong absorption between 500-700 nm associated with π–π^* electronic transition and spectral shape very similar to that of the corresponding results in the solution shown in the Fig. 4. It can also be seen that calculated values of λ_{max} as shown in the table 1 are a bit smaller as compared to the corresponding experimentally measured values in solution, which is because calculation has been done for the single molecule in gaseous state where intermolecular interactions are highly diminished as compared to the solution. In the meantime, SQ-90 and SQ-94 exhibit 4-8 nm red-shifted λ_{max} as compared to other dyes indicating the similar trend as measured experimentally. Therefore, such a precise and reliable predictions made by TD-DFT in present case ensures that functional and basis set selected for TD-DFT calculations are quite adequate.

3.3 Energy band diagram

Dye molecule adsorbed on the surface of TiO_2 gets excited from the ground state due to incident photons resulting from the intramolecular π-π^* electronic transition. The difference in the energy levels of two materials in contact usually is the reason for driving force for electron transfer (40). Therefore, sensitizers having higher energy level as compared to the TiO_2 conduction band (CB) are susceptible to the electron injection after the photoexcitation. As a result, dye molecule attains the oxidized state and needs to be reduced by electron transfer from redox couple (I^-/I_3^-) a process well known as dye regeneration (41). Therefore, an energetic cascade between the TiO_2, CB, dye molecules and redox couple is highly desired for the electron injection and dye regeneration. Utilizing combined theoretical and experimental approaches, we have recently demonstrated that it is possible to inject electrons from the excited dye molecules to the CB of TiO2 with minimum possible energy barrier as low as 0.15 eV [38]. In this work, unsymmetrical squaraine dyes have been logically designed in order to find the minimum possible energy barrier for regeneration of the excited dye molecules by redox electrolyte using most widely used I^-/I_3^- redox couple. In a typical DSSC, the dye regeneration efficiency is being controlled by the dye molecular structure and their HOMO energy level. The energy diagram for all of the dyes utilized along with the TiO_2 and I^-/I_3^- is shown in the Fig. 6.

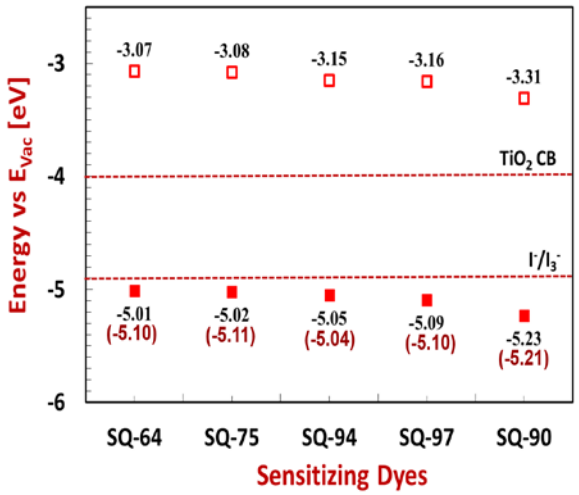

Figure 6. HOMO energy level by Photoelectron Yield Spectroscopy (PYS). Optical band gap (Eg) from on onset of absorption spectra LUMO = HOMO + Eg. Values in parenthesis are the theoretically calculated values of HOMO energy for squaraine dyes using TD-DFT.

Energy band diagram shown in the Fig. 6 was constructed by considering the redox potential of I_3^-/I^- redox couple to be 0.44 V vs. NHE or - 4.9 eV with respect to the vacuum level. [42]. On the other hand, CB of TiO_2 was taken to be - 4.0 eV considering the most negative quasi Fermi level corresponding to the flat band potential of TiO_2 (0.7 V vs. SCE) [43]. Energy level of dye molecules in this work exhibit the energetics having favourable energy levels with respect to the CB of TiO_2 and redox energy level of I_3^-/I^- redox couple ensuring the thermodynamic possibility of electron injection and dye regeneration. It is interesting to note that values of the HOMO energy level of dyes calculated using TD-DFT depicts very good similarity (only an error of 0.01-0.09 eV) with their corresponding experimentally measured values by PYS and further ensures the reliability of our theoretical prediction of the energetics. It can be clearly seen from the energy band diagram that the change in dye molecular structure has direct and significant impact on their energy levels. SQ-97 depicts its HOMO energy at -5.09 eV and LUMO energy at -3.16 eV, and a downward shift of energy levels was observed in case the of SQ-90 which could be associated with presence electron withdrawing -Br attached to the Indole ring (Fig. 1). Similarly, in the case of SQ-94 there was an upward shift in the energy levels due to presence of the electron donating $-OCH_3$ group. Squaraine dyes with long alkyl chains like SQ-75 and SQ-64 exhibited increase in their energy level as compared to the dyes with short alkyl chains reaching HOMO energy level very near to the I_3^-/I^- redox energy level with a minimum difference of 0.11 eV for SQ-64. Previously, we have also shown that there is an upward shift in the energy level of squaraine dyes as function of increasing alkyl chain length suggesting the possibility of fine turning of energetics by controlling the alkyl chain length [44].

3.4 Photovoltaic Characterizations

Good energetic matching between the unsymmetrical squaraine with respect to the CB of TiO2 and redox energy level of iodine based redox electrolyte as shown in the Fig. 6 encouraged us to investigate their photovoltaic characteristics. Another aim was to probe the minimum driving force required for the dye regeneration since we have already reported a minimum energy barrier of 0.16 eV for electron injection [38]. Figure 7 (a) depicts the photocurrent density-voltage (*J*-V) curve for the DSSCs based squaraine sensitizers measured under global AM 1.5G simulated solar illuminations. At the same time, photovoltaic parameters deduced from the J-V curves are summarized in the table-2. It can be clearly seen form this figure and table that DSSC fabricated using SQ-75 gave best photoconversion efficiency (PCE) of 4.25% having a short circuit current density (Jsc) of 10.92 mA/cm^2, open circuit voltage (Voc) of 0.57 V, and fill factor (FF) of 0.67. Amongst the dyes used, this dye SQ-75 exhibited both of highest Jsc and of Voc leading to the best PCE. The reason for high value of Jsc could be associated with the facile electron injection as well as dye regeneration. This was further supported by the very good photosensitization as confirmed by photocurrent action spectral measurement shown in the Fig. 7(b). In the action spectrum, dye SQ-75 exhibited a highest incident photon to current conversion efficiency (IPCE) of (~56%) mainly in the far-red wavelength peaking around 640 nm and could be responsible for the observation of the highest Jsc in the J-V characteristic amongst the dyes used as sensitizer in this work. Organic dyes typically bearing flat molecular structure are prone to dye aggregation and such dye aggregates especially blue-shifted H-aggregates exhibits hampered electron injection as compared to their monomeric dye counterparts [45]. This hampered electron injection due to dye aggregation leads to enhanced back electron transfer or charge recombination finally leading hampered Voc and PCE. Inoue et al demonstrated that symmetrical squaraine dyes with H-aggregates exhibits poor Jsc as well as poor Voc both finally leading to the hampered DSSC performance [46]. We have already discussed in the section 3.1 that H-aggregated squaraine dyes exhibit enhanced light absorption in lower wavelength (400-500 nm) region. SQ-75 does not show any absorption in this lower region even in the solid-state (Fig. 4). Therefore, such a least aggregation of SQ-75 dye molecules could attributed to the observed highest Voc, which was further supported by appreciable fluorescence lifetime (1.044 ± 0.005 ns) as shown in the table 1.

Table 2. Photovoltaic parameters for the DSSCs fabricated using unsymmetrical of squaraine dyes under simulated solar irradiation.

Sensitizing dyes	Jsc (mA/cm^2)	Voc (V)	FF	Efficiency (%)
SQ 64	8.7	0.54	0.64	3.08
SQ 75	10.92	0.57	0.67	4.25
SQ 90	9.84	0.55	0.64	3.52
SQ 94	7.3	0.51	0.63	2.4
SQ 97	9.25	0.53	0.67	3.3

In spite of nearly similar energetics, SQ-64 exhibits drastically hampered PCE of 3.08% (reduced Jsc and Voc), which might be due to increased charge recombination as confirmed by decrease in fluorescence lifetime (0.9478 ± 0.00423 ns). This increase in recombination could be associated with the hampered

electron injection into TiO_2 facilitated by H-aggregate formation. It is worth to mention here that SQ-97 and SQ-94 also exhibit pronounced dye aggregation as confirmed by solid-state electronic absorption spectra shown in the Fig. 4. Perusal of Table 2 and Fig. 7 (a) clearly indicate that DSSCs based on dyes SQ-97 and SQ-94 give poor efficiency of 3.3 % and 2.4 %, respectively. Presence of dye enhanced light absorption (Fig. 4) and clear peak in the action spectra (Fig. 7b) in the lower wavelength region (400-500 nm) might be responsible for the hampered PCE especially Voc. At the same time, relatively decreased lifetime for dyes SQ-97 and SQ-94 in ethanol solution with measured values of 0.904 ± 0.004 ns and 0.434 ± 0.076 ns, respectively, verify the possibility of relatively enhanced charge recombination leading lower Voc. It can be seen that by judicious molecular design we have demonstrated that fine control of HOMO energy level. It is interesting to note here that unsymmetrical squaraine dye SQ-75 exhibited highest PCE and best photon harvesting in the far-red region in spite of its very small energy difference of 0.12 with respect to the I_3^-/I^- redox energy level. Therefore, it clearly demonstrates that it is possible to have facile dye regeneration with a small driving force as low as of 0.12 eV. Combining this newly obtained result on minimum energy barrier for dye regeneration (0.12 eV) with the our result on estimation minimum driving force required for electron injection (0.16 eV) [38], it can be concluded that is practically possible to design and develop novel sensitizers having an energy band gap of 1.18 eV. Such newly designed sensitizers could be utilized for the fabrication of high efficiency DSSCs using mesoporous TiO_2 as dye adsorption scaffold and I_3^-/I^- redox electrolyte having capability of photon harvesting up to 1050 nm.

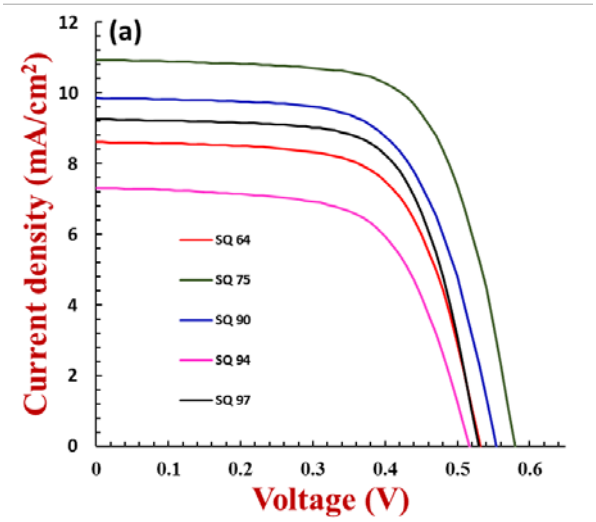

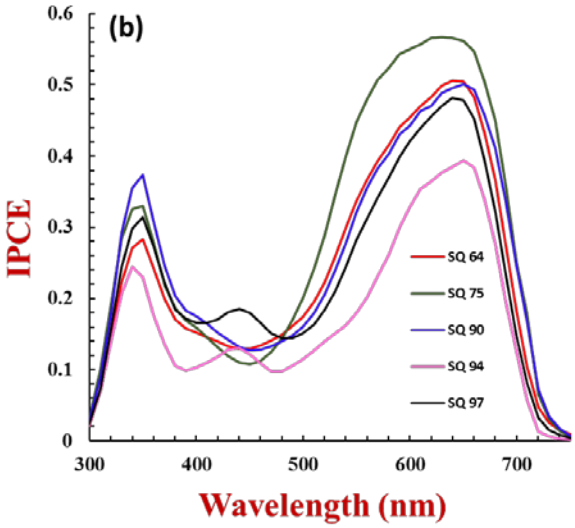

Fig. 7 J-V plot for DSSCs using squaraine dyes under simulated solar irradiation (a) and photocurrent action spectra after monochromatic light illumination (b).

Conclusions

Far-red sensitive unsymmetrical squaraine dyes were logically designed successfully synthesized using combined theoretical and experimental approached in order to probe the minimum driving force for dye regeneration. It has been demonstrated that only slight positional variation of long alkyl substituents while keeping the same p-molecular framework (SQ-64 and SQ-75) led to drastic differences in their photovoltaic performances, which was explained by their differential aggregation behavior. It has been shown that use of LSDA functional under DFT predicts the energetics and electronic absorption spectrum of squaraine dyes under investigation very well. Calculated values of HOMO energy level of dyes exhibit only an error of 0.01-0.09 eV with their corresponding experimentally measured values by PYS and validates the reliability of our theoretical prediction of the energetics. Highest photon harvesting exhibited by SQ-75 clearly corroborates the possibility of facile dye regeneration with a minimum energy of 0.12 eV with respect to the most commonly employed I^-/I_3^- redox electrolytes. In combination with the minimum energy barrier needed for electron injection published by our group earlier, current result on need of minimum driving force 0.12 eV for dye regeneration indicates the possibility of novel dye design having the capability of photon harvesting up 1050 nm.

Acknowledgements

Authors are thankful for the financial support by JSPS grant-in-aid for scientific research-C (Grant number-26410206) to carry out this research work and is being gratefully acknowledged.

Notes and references

1. H. Lund and B. V. Mathiesen, *Energy*, 2009, **34**, 524-531.
2. A. M. Omer, *Journal of Agricultural Extension and Rural Development*, 2010, **2**, 001-021.
3. H. S. Jung and J.-K. Lee, *The journal of physical chemistry letters*, 2013, **4**, 1682-1693.

4. A. Nattestad, A. J. Mozer, M. K. Fischer, Y.-B. Cheng, A. Mishra, P. Bäuerle and U. Bach, *Nature materials*, 2010, **9**, 31-35.
5. F. Odobel and Y. Pellegrin, *The Journal of Physical Chemistry Letters*, 2013, **4**, 2551-2564.
6. A. Mishra, M. K. Fischer and P. Bäuerle, *Angewandte Chemie International Edition*, 2009, **48**, 2474-2499.
7. J.-H. Yum, E. Baranoff, F. Kessler, T. Moehl, S. Ahmad, T. Bessho, A. Marchioro, E. Ghadiri, J.-E. Moser and C. Yi, *Nature communications*, 2012, **3**, 631.
8. Z. Shi, K. Deng and L. Li, *Scientific reports*, 2015, **5**, 9317.
9. M. K. Nazeeruddin, F. De Angelis, S. Fantacci, A. Selloni, G. Viscardi, P. Liska, S. Ito, B. Takeru and M. Grätzel, *Journal of the American Chemical Society*, 2005, **127**, 16835-16847.
10. M. Grätzel, *Accounts of chemical research*, 2009, **42**, 1788-1798.
11. A. Islam, M. Akhtaruzzaman, T. H. Chowdhury, C. Qin, L. Han, I. M. Bedja, R. Stalder, K. S. Schanze and J. R. Reynolds, *ACS applied materials & interfaces*, 2016, **8**, 4616-4623.
12. Y. Ogomi, S. S. Pandey, S. Kimura and S. Hayase, *Thin Solid Films*, 2010, **519**, 1087-1092.
13. M. Kimura, H. Nomoto, N. Masaki and S. Mori, *Angewandte Chemie International Edition*, 2012, **51**, 4371-4374.
14. S. Y. Chae, S. J. Park, O.-S. Joo, Y. Jun, B. K. Min and Y. J. Hwang, *Scientific reports*, 2016, **6**, 30868.
15. T. W. Hamann, R. A. Jensen, A. B. Martinson, H. Van Ryswyk and J. T. Hupp, *Energy & Environmental Science*, 2008, **1**, 66-78.
16. A. Mishra, M. K. Fischer and P. Bäuerle, *Angewandte Chemie International Edition*, 2009, **48**, 2474-2499.
17. S. S. Pandey, T. Inoue, N. Fujikawa, Y. Yamaguchi and S. Hayase, *Journal of Photochemistry and Photobiology A: Chemistry*, 2010, **214**, 269-275.
18. S. S. Pandey, T. Inoue, N. Fujikawa, Y. Yamaguchi and S. Hayase, *Thin Solid Films*, 2010, **519**, 1066-1071.
19. S. Kim, J. K. Lee, S. O. Kang, J. Ko, J.-H. Yum, S. Fantacci, F. De Angelis, D. Di Censo, M. K. Nazeeruddin and M. Grätzel, *Journal of the American Chemical Society*, 2006, **128**, 16701-16707.
20. N. N. Matsuzawa, A. Ishitani, D. A. Dixon and T. Uda, *The Journal of Physical Chemistry A*, 2001, **105**, 4953-4962.
21. W. Pham, W.-F. Lai, R. Weissleder and C.-H. Tung, *Bioconjugate chemistry*, 2003, **14**, 1048-1051.
22. S. S. Pandey, R. Watanabe, N. Fujikawa, Y. Ogomi, Y. Yamaguchi and S. Hayase, 2011.
23. T. Morimoto, N. Fujikawa, Y. Ogomi, S. S. Pandey, T. Ma and S. Hayase, *Journal of nanoscience and nanotechnology*, 2016, **16**, 3282-3288.
24. M. Matsui, T. Yamamoto, Y. Kubota and K. Funabiki, *New Journal of Chemistry*, 2016, **40**, 10187-10196.
25. H. Li, M. Pang, B. Wu and J. Meng, *Journal of Molecular Structure*, 2015, **1087**, 73-79.
26. M. Saikiran, D. Sato, S. Pandey and T. Kato, 2016.
27. A. Levitz, S. T. Ladani, D. Hamelberg and M. Henary, *Dyes and Pigments*, 2014, **105**, 238-249.
28. S. Sreejith, P. Carol, P. Chithra and A. Ajayaghosh, *Journal of Materials Chemistry*, 2008, **18**, 264-274.
29. E. Soriano, C. Holder, A. Levitz and M. Henary, *Molecules*, 2015, **21**, 23.
30. A. Levitz, S. T. Ladani, D. Hamelberg and M. Henary, *Dyes and Pigments*, 2014, **105**, 238-249.
31. M. J. Marchena, G. de Miguel, B. Cohen, J. A. Organero, S. Pandey, S. Hayase and A. Douhal, *The Journal of Physical Chemistry C*, 2013, **117**, 11906-11919.
32. J.-H. Yum, P. Walter, S. Huber, D. Rentsch, T. Geiger, F. Nüesch, F. De Angelis, M. Grätzel and M. K. Nazeeruddin, *Journal of the American Chemical Society*, 2007, **129**, 10320-10321.
33. J. Yum, S. Moon, R. Humphry-Baker, P. Walter, T. Geiger, F. Nüesch, M. Grätzel and M. d K Nazeeruddin, *Nanotechnology*, 2008, **19**, 424005.
34. Y.-S. Kim, K. Liang, K.-Y. Law and D. G. Whitten, *The Journal of Physical Chemistry*, 1994, **98**, 984-988.
35. Y. Xu, Z. Li, A. Malkovskiy, S. Sun and Y. Pang, *The Journal of Physical Chemistry B*, 2010, **114**, 8574-8580.
36. M. Pastore, S. Fantacci and F. De Angelis, *The Journal of Physical Chemistry C*, 2013, **117**, 3685-3700.
37. M. K. Nazeeruddin, F. De Angelis, S. Fantacci, A. Selloni, G. Viscardi, P. Liska, S. Ito, B. Takeru and M. Grätzel, *Journal of the American Chemical Society*, 2005, **127**, 16835-16847.
38. S. S. Pandey, T. Morimoto, N. Fujikawa and S. Hayase, *Solar Energy Materials and Solar Cells*, 2017, **159**, 625-632.
39. R. Sánchez-de-Armas, M. Á. San Miguel, J. Oviedo and J. F. Sanz, *Physical Chemistry Chemical Physics*, 2012, **14**, 225-233.
40. D. Cahen, G. Hodes, M. Grätzel, J. F. Guillemoles and I. Riess, *The Journal of Physical Chemistry B*, 2000, **104**, 2053-2059.
41. G. Boschloo and A. Hagfeldt, *Accounts of chemical research*, 2009, **42**, 1819-1826.
42. Y. Ogomi, T. Kato and S. Hayase, *Journal of Photopolymer Science and Technology*, 2006, **19**, 403-408.
43. A. Hagfeldt and M. Graetzel, *Chemical Reviews*, 1995, **95**, 49-68.
44. S. S. Pandey, T. Inoue, N. Fujikawa, Y. Yamaguchi and S. Hayase, *Journal of Photochemistry and Photobiology A: Chemistry*, 2010, **214**, 269-275.
45. A. C. Khazraji, S. Hotchandani, S. Das and P. V. Kamat, *The Journal of Physical Chemistry B*, 1999, **103**, 4693-4700.
46. T. Inoue, S. S. Pandey, N. Fujikawa, Y. Yamaguchi and S. Hayase, *Journal of Photochemistry and Photobiology A: Chemistry*, 2010, **213**, 23-29.